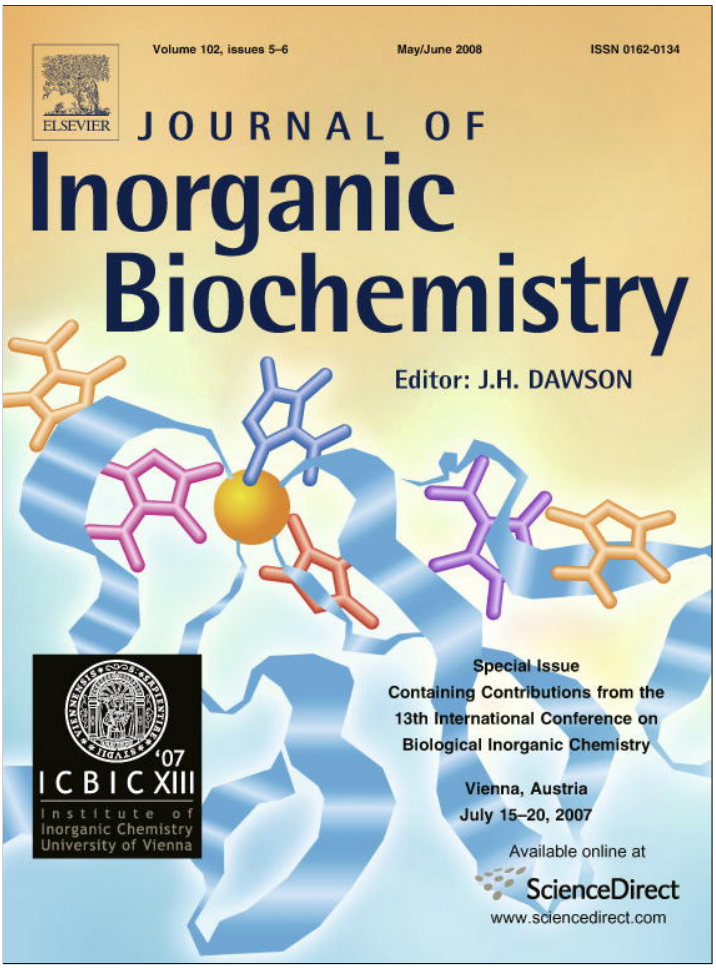

Available online at www.sciencedirect.com
ScienceDirect
Journal of Inorganic Biochemistry 102 (2008) 1322–1328
Journal of Inorganic Biochemistry
www.elsevier.com/locate/jinorgbio

High resolution crystal structure of *Rubrivivax gelatinosus* cytochrome *c′*

Stefano Benini [a,e], Wojciech R. Rypniewski [b], Keith S. Wilson [a], Stefano Ciurli [c,d,*]

[a] *York Structural Biology Laboratory, Department of Chemistry, University of York, Heslington, York, YO10 5YW, United Kingdom*
[b] *Institute of Bioorganic Chemistry, Polish Academy of Sciences, Noskowskiego 12/14, 61-704 Poznan, Poland*
[c] *Laboratory of Bioinorganic Chemistry, Department of Agro-Environmental Science and Technology, University of Bologna, Viale Giuseppe Fanin 40, 40127 Bologna, Italy*
[d] *CERM (Center for Magnetic Resonance), Via Luigi Sacconi 6, 50019 Sesto Fiorentino, Firenze, Italy*
[e] *Present address: AstraZeneca, Mereside, Alderley Park, Macclesfield, SK10 4TG, Cheshire, England, United Kingdom*

Received 25 September 2007; received in revised form 6 January 2008; accepted 8 January 2008
Available online 21 January 2008

Abstract

The structure of the cytochrome *c′* from the purple non-sulfur phototrophic bacterium *Rubrivivax gelatinosus* was determined using two crystals grown independently at pH 6.3 and pH 8. The resolution attained for the two structures (1.29 Å and 1.50 Å for the crystals at high and low pH, respectively) is the highest to date for this class of proteins. The two structures were compared in detail in an attempt to investigate the influence of pH on the geometry of the haem and of the coordination environment of the Fe(III) ion. However, while the results suggest some small propensity for the movement of the metal atom out of the plane of the haem ring upon pH increase, the accuracy of the measurements at these two pH below the p*K* of the axial histidine is not sufficient to provide hard evidence of a shift in the iron position and associated changes.

Keywords: Cytochrome *c′*; *Rubrivivax gelatinosus*; X-ray crystallography; Electronic structure; Electron transfer

1. Introduction

Cytochromes *c′* are found in phototrophic [1,2], denitrifying [3], nitrogen-fixing [4], methanotrophic [5] and sulfur-oxidizing [6] bacteria [7]. Their physiological function is still unclear: while a role in electron transfer has been suggested on the basis of their redox properties [8], a function in NO resistance has also been proposed [9]. The X-ray structures of native ferric cytochrome *c′* are available from *Chromatium* (*Ch.*) *vinosum* (PDB code 1BBH, 1.80 Å resolution) [10], *Rhodospirillum* (*Rs.*) *molischianum* (PDB code 2CCY, 1.67 Å) [11], *Rhodobacter* (*Rb.*) *capsulatus* (PDB codes 1RCP, 1CPQ, and 1CPR, at 2.00, 1.72, and 1.72 Å, respectively) [12–14], *Rhodopseudomonas* (*Rps.*) *palustris* (PDB code 1A7V, 2.30 Å), *Rhodobacter* (*Rb.*) *sphaeroides* (PDB code 1GQA, 1.80 Å) [15], *Rubrivivax* (*Rv.*) *gelatinosus* (PDB code 1JAF, 2.50 Å) [16], and several species of *Alcaligenes* (PDB codes 1CGN, 1CGO, and 1E83 at 2.15 Å, [17], 1.80 Å, [17], and 2.05 Å, [18], respectively). These structures reveal that cytochromes *c′* are generally characterized by a four-helix bundle structural motif, by covalent attachment of the haem to a conserved CXXCH sequence pattern, and by the presence of a penta-coordinated Fe(III) ion, axially bound to a solvent-exposed His residue. The sixth coordination site, pointing toward the protein core, is empty and tightly packed by the surrounding aromatic and hydrophobic amino acid residues. Cytochromes *c′* are usually isolated as soluble homodimers, each subunit being ca. 14 kDa. Only the protein isolated from *Rps. palustris* is a monomer, while in the case of *Rb. capsulatus* and *Rb. sphaeroides* a mixture of monomers and dimers is obtained [19,20].

* Corresponding author. Address: Laboratory of Bioinorganic Chemistry, Department of Agro-Environmental Science and Technology, University of Bologna, Viale Giuseppe Fanin 40, 40127 Bologna, Italy. Tel.: +39 051 209 6204; fax: +39 051 209 6203.
E-mail address: stefano.ciurli@unibo.it (S. Ciurli).

0162-0134/$ - see front matter © 2008 Elsevier Inc. All rights reserved.
doi:10.1016/j.jinorgbio.2008.01.017

Cytochromes c' have peculiar spectroscopic and magnetic properties [21]. In particular, the spin state of the ferric cytochrome c' has been the subject of controversy. Generally, Fe(III) ions in haem-containing proteins can exist in any of the three ground spin states schematically shown in Fig. 1. The $S = 1/2$ low spin state is commonly found when two axial ligands complete the coordination environment of the haem ferric ion, and are characterized by an energy separation between the d(xy, xz) and d(z^2) orbitals, Δ_1, larger than the spin pairing energy, P. When the Δ_1 energy gap is smaller than P, there are two possibilities: (i) if $P < \Delta_2$, the energy gap between the d$(x^2 - y^2)$ and the d(z^2) orbitals, then the intermediate spin state $S = 3/2$ is obtained, while (ii) if $\Delta_2 <$ P the high-spin state $S = 5/2$ is produced. While several cases of $S = 3/2$ haem model complexes and many high-spin ferric haem proteins with five-coordinate haem Fe(III) ion are known, no examples of haem proteins in a pure mid-spin state are currently available [21]. Early magnetic susceptibility measurements on cytochromes c' were interpreted with a physical model that implied a thermal equilibrium between the low spin ($S = 1/2$) and the high-spin ($S = 5/2$) states [22]. Later, optical [23], near infrared [24], near infrared MCD [25], Mössbauer [26], and NMR [27–32] data suggested that cytochrome c' is substantially high-spin ($S = 5/2$) at neutral pH. In contrast to both hypotheses above, EPR [33–40], Mössbauer [41], optical [42], NMR [43] and resonance Raman [44] results were interpreted with the hypothesis of a quantum mechanical admixture of a high-spin ($S = 5/2$) and an intermediate spin ($S = 3/2$) state. This peculiar quantum state can theoretically be obtained when the energy separation between the $S = 3/2$ and $S = 5/2$ states is of the order of kT at ambient temperature [21]. Based largely on EPR data, it appears that the contribution of the intermediate spin state depends on the bacterial source from which the cytochrome c' is derived, ranging from approximately 10% to 60% [33–40]. Cytochromes c' from *Rps. palustris*, *Rb. capsulatus*, and *Ch. vinosum* appear to have a larger contribution of the $S = 3/2$ state (40–60%), while cytochromes c' from *Rs. rubrum*, *Rs. molischiatum*, and *A. xylosoxidans* seem to have a much smaller intermediate spin contribution (10–15%). For *Rps. palustris*, and in contrast to the EPR studies above, resonance Raman spectroscopy suggested that the $S = 3/2$ state constitutes essentially 100 % of the electronic ground state [44], while for cytochromes c' from *Rs. molischiatum* and *Rs. rubrum* EXAFS studies suggested a much larger mid-spin contribution than expected from the EPR data [5]. According to the theoretical model for quantum mechanical spin-admixtures the relative contribution of $S = 3/2$ and $S = 5/2$ states to the ground state varies depending on Δ_2 (Fig. 1): when Δ_2 increases, the contribution of $S = 3/2$ increases, while when Δ_2 decreases, the contribution of $S = 5/2$ increases. In turn, this depends on the energies of the d$(x^2 - y^2)$ and d(z^2) orbitals: as the energy of d$(x^2 - y^2)$ decreases and that of d(z^2) increases, the ground state will change from predominantly $S = 3/2$ to predominantly $S = 5/2$.

In cytochromes c', the contribution of the intermediate spin state to the ground state also appears to depend on the pH of the solution, decreasing as the pH increases, resulting in a high-spin ferric ion at pH 11.0 [22,23,25,33,35,40,45]. NMR spectroscopic studies, carried out on the Fe(III) form of the protein in order to elucidate the molecular basis for this pH-modulated transition, have revealed the presence of three pK_a values: 5.3, 6.7, and 8.8 for *Ch. vinosum* cytochrome c' [30,31] and 4.8, 6.7, and 9.0 for *Rv. gelatinosus* cytochrome c' [32]. The first two pK_a's have been assigned to the two propionic carboxylate residues of the haem moiety, while the third pK_a, causing a much larger spectral shift, has been tentatively attributed to the deprotonation of the Nδ1 of the proximal histidine ligand. Deprotonation of the axial histidine could cause the formation of a strong anionic ligand and the consequent displacement of Fe(III) from the haem plane: this process would cause a destabilization of d(z^2) and a stabilization of d$(x^2 - y^2)$, and therefore a transition from a state in which $S = 3/2$ has a large contribution to the spin-admixed state, to a situation in which the ground state is essentially high-spin $S = 5/2$ (Fig. 1).

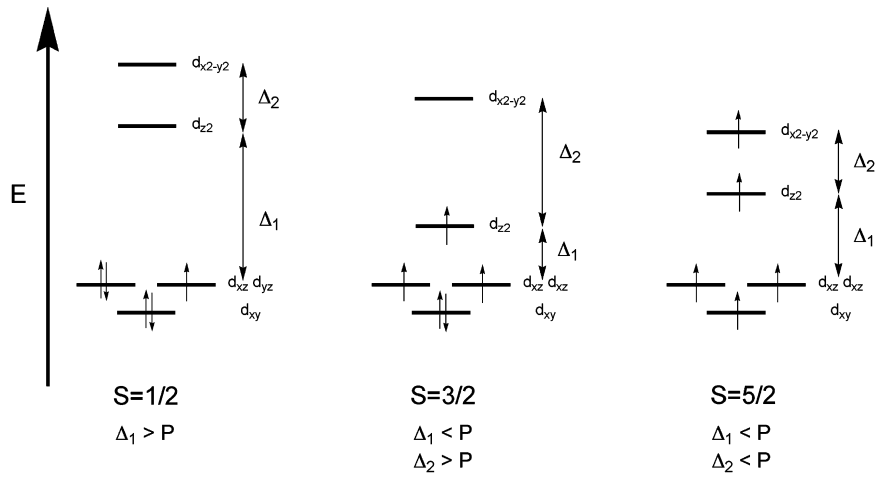

Fig. 1. Schematic distribution of d-orbitals giving rise to different electronic spin ground state in Fe(III) heme proteins.

We report here on a study of the structure of a cytochrome c' carried out in order to push the resolution as high as possible, and we have succeeded in determining the structure of the protein from *Rv. gelatinosus* at 1.50 and 1.29 Å, from crystals grown at pH 6.3 and 8.0, respectively, using cryogenic conditions and synchrotron radiation. The availability of these structures allowed us to analyze and discuss the biophysical properties of this family of proteins.

2. Materials and methods

2.1. Protein purification and crystallization

Rubrivivax gelatinosus (DSM, Deutsche Sammlung von Mikroorganismen, Göttingen, Germany, type strain 1709) was grown at 25 °C under photoheterotrophic conditions (medium 27, DSM). *Rv. gelatinosus* cytochrome c' was isolated and purified in the oxidized state following the procedure described by Bartsch [46]. Purity was checked by SDS–PAGE electrophoresis.

Protein crystallization trials on the freshly purified *Rv. gelatinosus* cytochrome c' were performed at 20 °C by the hanging drop method, using 5 μL of a 20 mg/mL protein solution in 20 mM Tris · HCl, pH 8, and diluting this volume with 5 μL of precipitant solution. The drop was equilibrated by vapour diffusion against 1 mL of precipitant solution using a Hampton Research 24-well Linbro plate. The initial screening for determination of the crystallization conditions was carried out as previously described [47]. In particular, two precipitant solutions gave single crystals of approximate dimensions $2.0 \times 2.0 \times 0.8$ mm, which were suitable for diffraction data collection: (i) 100 mM Tris · HCl, pH 8.0, containing 2.5 M ammonium sulfate, and (ii) 100 mM sodium citrate, pH 6.3, containing 2.5 M ammonium sulfate. The crystals obtained in these two conditions will be referred to as Crystal-6 and Crystal-8, to distinguish them on the basis of the pH at which they were obtained.

2.2. Crystallographic diffraction data collection and evaluation

The crystals were transferred from the mother liquor to the cryobuffer (20% glycerol in the precipitant solution), scooped up in a rayon cryoloop, and rapidly exposed to a cold nitrogen stream (Oxford Cryosystem) on the BW7B (Crystal-6) and X11 (Crystal-8) beam lines, respectively, of the DORIS storage ring at the EMBL outstation at the Deutsches Elektronen Synchrotron (DESY) in Hamburg (Germany). Diffraction data were collected at 100 K using a 30-cm MAR Research imaging plate scanner (Hamburg, Germany). One single crystal was used to record the entire data set in three sweeps, at different exposure times. The pH of the cryobuffer was checked, and multiple measurements confirmed that addition of glycerol did not alter the pH of the buffer used for the crystallization.

The images were processed with DENZO and merged with SCALEPACK [48]. For both crystals, *Rv. gelatinosus* cytochrome c′ crystallizes in the trigonal space group $P3_121$, with two molecules (14 kDa) per asymmetric unit. The calculated volume-to-mass ratio ($V_M = 3.1$ Å^3/Da) and solvent content of the crystal (60%) are in the normal range found for proteins [49]. Table 1 reports a summary of data collection procedures, data statistics, and the results of data analysis for *Rv. gelatinosus* cytochrome c′.

2.3. Structure determination and refinement

All computations were carried out with programs from the CCP4 package [50] unless otherwise stated. The structure of Crystal-8 was solved by the molecular replacement technique as implemented in the program AMoRe [51], using the structure of *Rv. gelatinosus* cytochrome c' [16] (PDB code: 1JAF) as a search model. The highest peak in the rotation function gave a correlation coefficient of 17.7%, and the translation search gave a clear solution of the structure with a correlation coefficient of 46.8%.

The model was first subjected to rigid body refinement and subsequently refined using REFMAC [52,53]. Randomly selected reflections (2% of the total) were used as an R_{free} set for cross validation. Ideal geometric parameters of the protein and haem group were those of Engh and Huber [54], while no restraints were used on the Fe atom position, nor on distances and angles between the Fe atom and its coordinating atoms. The parameters refined were the atomic positions and the isotropic B-factors of non-hydrogen atoms. The protein regions displaying different conformations were manually rebuilt with the program O [55]. Automatic solvent building was performed using the program ARP [56], keeping only those water molecules having density greater than 0.5σ in the 2Fo−Fc electron density map. The high resolution of the data allowed an anisotropic refinement. Positions of hydrogen atoms were

Table 1
Summary of X-ray data collection statistics and data reduction for *Rubrivivax gelatinosus* cytochrome c'

pH	6.3	8.0
PDB code	2J9B	2J8W
Wavelength (Å)	0.84	0.91
Resolution range (Å)	19.92–1.50	19.96–1.29
High resolution bin (Å)	1.53–1.50	1.31–1.29
Number of reflections	547519	445489
Unique reflections	55765	87744
Redundancy	9.8	5.1
% Completeness (high resolution bin)	99.4 (99.2)	99.8 (99.3)
% R_{sym} (high resolution bin)	4.7 (22.5)	4.4 (38.5)
I/σ (high resolution bin)	33 (8.2)	14 (3.6)
% Greater than 3σ (high resolution bin)	92.7 (77.3)	79.7 (48.5)
Space group	$P3_121$	$P3_121$
$a = b$ (Å)	69.56	69.63
c (Å)	123.37	123.63

Table 2
Summary of crystallographic data analysis for *Rv. gelatinosus* cytochrome *c′*

pH	6.3	8.0
PDB code	2J9B	2J8W
Protein atoms	1910	1998
Solvent atoms	460	562
B-Factor from Wilson plot	19.79	19.43
Temperature factors for main chain protein atoms (Å^2)	19.40 (chain A) 18.37 (chain B)	18.20 (chain A) 15.84 (chain B)
Temperature factors for side chain protein atoms (Å^2)	21.00 (chain A) 19.84 (chain B)	19.52 (chain A) 17.75 (chain B)
Temperature factors for Fe atom (Å^2)	16.45 (chain A) 15.45 (chain B)	15.37 (chain A) 13.90 (chain B)
Temperature factors for solvent atoms (Å^2)	34.62	34.81
RMSD bond length variation (Å)	0.015	0.017
RMSD bond angle variation (degrees)	1.65	1.78
Ramachandran most favored region (%)	95.3	94.9
Ramachandran additional allowed region (%)	4.7	5.1
Ramachandran generously allowed region (%)	0	0
R_{factor} (%)	14.9	14.4
R_{free} (%)	17.8	17.2

calculated before each maximum likelihood refinement cycle, and their contribution to the structure factors was added to the structure factors calculated from the model. The stereochemistry of the final model for the two structures was checked using the program PROCHECK [57]. The final statistics for the structures are summarized in Table 2.

The refined crystallographic coordinates and structure factors have been deposited in the Protein Data bank with the accession codes 2J9B (pH 6.3) and 2J8W (pH 8.0).

3. Results and discussion

Rubrivivax gelatinosus cytochrome *c′* consists of a homodimer with each subunit composed of an elongated left-twisted bundle made of four anti-parallel α-helices, named I–IV, typical for this family of proteins (Fig. 2A). Helices I and II are connected by a short loop made of residues 32–36, while helices III and IV form a kink involving residue Asp104. A longer loop, formed by residues 59–73, connects helices II and III, and is located on the opposite side of the short loop and the kink. There are no substantial differences in the overall protein architecture and fold between the structures at pH 6.3 and 8.0, nor with the previously reported lower resolution structure (PDB code 1JAF): the root-mean-square deviation of the backbone atoms between the lower resolution structure (PDB code 1JAF) and those at pH 6.3 and 8.0 are 0.27 Å in both cases. The homodimer is formed by the two subunits almost at right angles to one other (Fig. 2B). No significant differences in the subunit–subunit association are observed with respect to the 1JAF structure.

As in all class-II *c*-type cytochromes, *Rv. gelatinosus* cytochrome *c′* is characterized by the presence of a haem group attached near the C-terminal region of the chain, by axial ligation to an imidazole ring of a solvent-exposed proximal histidine, and by the absence of a second axial ligand (Figs. 2 and 3). It was hoped that the analysis of the haem environment in the two crystals grown independently from solutions at pH 6.3 and 8.0, together with the reported pK_a values for this protein (4.8, 6.7, and 9.0 Bertini et al. [32]) and with the high quality of the crystal-

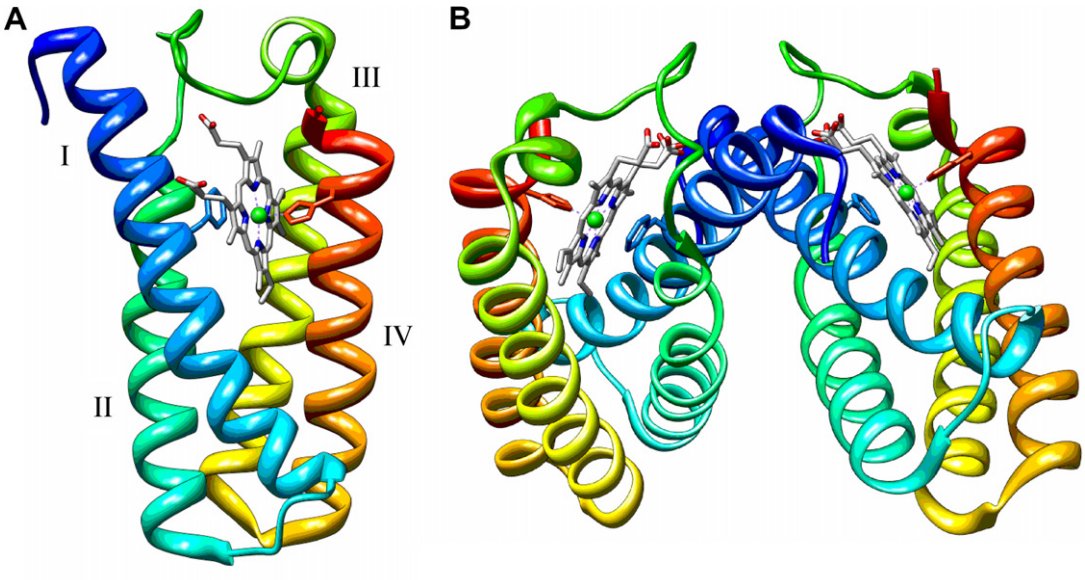

Fig. 2. A. Ribbon scheme of *Rv. gelatinosus* cytochrome *c′* monomer (PDB code 2J8W), coloured according to a rainbow code (blue: N-term, red: C-term). The axial His123 and the proximal Phe16 are shown as sticks, while the haem group is coloured according to CPK code; B. Ribbon scheme of the *Rv. gelatinosus* cytochrome *c′* dimer. Helices I–IV are indicated.

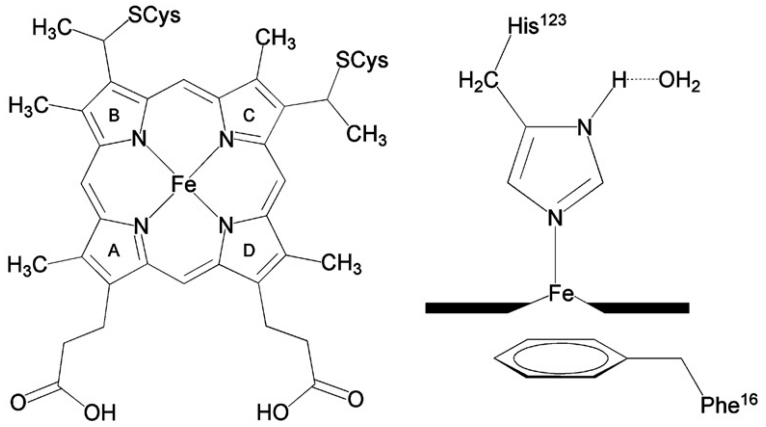

Fig. 3. Scheme of the *c*-type haem group (left panel) and of the spatial arrangement of the Fe(III) ligands with respect to the haem mean plane.

Table 3
Coordination distances of the haem Fe(III) ion

	pH 6.3	pH 8.0
Fe–N_A (Å)	2.03 (chain A)	2.01 (chain A)
	2.03 (chain B)	2.04 (chain B)
Fe–N_B (Å)	2.08 (chain A)	2.06 (chain A)
	2.07 (chain B)	2.07 (chain B)
Fe–N_C (Å)	2.03 (chain A)	1.97 (chain A)
	2.04 (chain B)	2.03 (chain B)
Fe–N_D (Å)	2.06 (chain A)	2.05 (chain A)
	2.09 (chain B)	2.07 (chain B)
Fe–N(His^{123}) (Å)	2.13 (chain A)	2.15 (chain A)
	2.14 (chain B)	2.11 (chain B)
Fe–N_4 displacement (Å)	0.21 (chain A)	0.24 (chain A)
	0.21 (chain B)	0.25 (chain B)
N_4–N(His^{123}) displacement (Å)	2.34 (chain A)	2.39 (chain A)
	2.35 (chain B)	2.35 (chain B)
N(His^{123})···O(wat)	3.41 (chain A)	3.30 (chain A)
	3.53 (chain B)	3.50 (chain B)

lographic data, would allow us to evaluate the pH-induced structural changes responsible for the pH-dependent spectroscopic properties (Table 3). In particular, our attention focused on the H-bonding networks involving the two haem propionate carboxylate side chains, connected to the indole rings A and D of the haem group, and the axially bound histidine residue, as well as on the Fe(III) ion displacement from the mean haem plane, as a function of pH. In addition, considering the lack of crystal symmetry between the two subunits in the homodimer, we considered the two haem groups in the two subunits, henceforth haem A and haem B, independently.

At pH 6.3, the O1D carboxylate oxygen of the propionate carboxylate group attached to ring D of both haem A and B receives H-bonds from Thr69 OHγ and from Arg12 NεH and Arg12 NH_2, while the O2D atom receives an H-bond from Glu70 NH and from Gln13 NεH, and is also at H-bonding distance from a water molecule (W163). This situation is the same at pH 8.0, indicating that this buried haem propionate chain is not affected by this pH increase. This group was suggested to determine the very minor NMR spectral perturbation occurring with a pK_a of 6.7 [32], and the present crystallographic evidence concurs with this interpretation: if there is a pH-induced change, this modification does not involve the making or breaking of H-bonds but rather a slight rearrangement of the same H-bond network. The situation is different for the propionate group attached to ring A, which forms extended H-bonding networks only with water molecules, and not with protein residues, because of its much larger exposure to bulk solvent. This chain adopts different conformations in haem B at pH 6.3 and of both haem A and haem B at pH 8.0. This solvent-mediated H-bonding network involves the carboxylate group of Glu70, a residue proposed, on the basis of NMR evidence, to modulate the pH-dependent properties of *Rv. gelatinosus* cytochrome *c′* with a pK_a of 4.8 [32].

Next, our attention shifts to the structural properties of the proximal axial residue, His123, as a function of pH: partial deprotonation of this residue would cause the formation of a strong anionic ligand, a condition that could lead to a displacement of the Fe(III) ion from the haem mean plane. In model complexes it is well-established that increasing this structural parameter from ca. 0.1 to ca. 0.5 Å induces a modification of the electronic ground state from a spin admixture of $S = 3/2$ and $S = 5/2$ states, in which the $S = 3/2$ contribution is large, to a situation described as an essentially pure high-spin, $S = 5/2$. This is because the displacement of the Fe(III) ion from the mean haem plane mainly causes a decrease of the energy of the d($x^2 - y^2$) orbital, whose lobes point directly to the four haem pyrrole nitrogen atoms, while the transformation of the neutral axial histidine into its anionic form induces an increase of the energy of the d(z^2) orbital. Overall, these two processes decrease the Δ_2 energy gap (see Fig. 1), in turn increasing the high-spin character of the electronic ground state and decreasing the contribution of the mid-spin electronic configuration. This hypothesis, certainly valid in model porphyrin complexes where there is a clear correlation between spin state of the haem iron and the Fe displacement from the mean haem plane [40], has

not been proven in proteins, reflecting the limited resolution of the X-ray structures available for cytochromes c'. In the present structures this displacement consistently shows a small increase with pH, from 0.21 to 0.24 Å for haem A, and from 0.21 to 0.25 Å for haem B, thus ranging between 0.03 and 0.04 Å (Table 3). This displacement may indicate an incipient process of total deprotonation of the axial histidine, known to occur at a pH 9.0 for this protein [32], as compared to the 6.3–8.0 range explored in the present study (attempts to obtain crystals at pH > 8 were unsuccessful). In order to establish the statistical significance of the apparent differences in structural parameters, in particular focusing on atomic distances, the estimated standard uncertainty (esu) in atomic positions were calculated for the models refined against all data, based on maximum likelihood and according to REFMAC [53]. The calculated values are 0.023 and 0.019 Å for the structure at pH 6.3 and 8.0, respectively. These values represent the statistical average of all the distances in the structure, and, for well-ordered atoms (such as the haem residue and the bound Fe), the uncertainty is expected to be somewhat lower. However the result suggests that the apparent movement in the iron position is close to the error in measurement at this resolution and does not provide strong evidence for a significant movement.

Analysis of the pH-induced changes affecting the H-bonding network of the axial histidine residue indicates that in both haem A and haem B, and at both pH 6.3 and 8.0, there is an H-bond between the His123 Nδ1 and a water molecule, and a slight decrease of the N···O(wat) distance is observed, from 3.41 to 3.30 Å for haem A and from 3.53 to 3.50 Å for haem B, upon pH increase from 6.3 to 8.0. This is consistent with a partial deprotonation of the solvent-exposed axial His123, again consistent with the reported $pK_a = 9.0$ for this process in *Rv. gelatinosus*.

In conclusion, this study provides the highest resolution structures to date of a cytochrome c'. The crystals were grown from drops set up at two different pH values: 6.3 and 8.0. The differences between the two structures are unfortunately too small to provide hard evidence for a relationship involving Fe displacement from the haem plane, axial histidine deprotonation, and increase of the percentage of the high-spin ($S = 5/2$) contribution to the spin-admixture of high and intermediate ($S = 3/2$). This may partly reflect that both crystals were one or pH units below the expected pK (9.0) of the key axial histidine, and that the accuracy of the X-ray models is still limiting even at this very high resolution.

4. Abbreviations

Ch *Chromatium*
Rs *Rhodospirillum*
Rb *Rhodobacter*
Rps *Rhodopseudomonas*
Rv *Rubrivivax*
A *Alcaligenes*
MCD magnetic circular dichroism
EXAFS extended X-ray absorption fine Structure
EMBL European Molecular Biology Laboratory

Acknowledgments

The authors thank the European Union for support of the work at EMBL Hamburg through the HCMP Access to Large Installation Project, Contract Number CHGE-CT93-0040. S.C. is grateful to the Ministero Italiano dell'Universita' e della Ricerca (MIUR) for partially funding this research.

References

[1] R.G. Bartsch in: R. Clayton, W. Sistrom (Eds.), The Photosynthetic Bacteria, Plenum, New York, 1978, pp. 249–280.
[2] T. Meyer, M. Kamen, Adv. Prot. Chem. 35 (1982) 105–212.
[3] H. Iwasaki, T. Yoshimura, S. Suzuki, S. Shidara, Biochim. Biophys. Acta 1058 (1991) 79–82.
[4] T. Yamanaka, S. Imai, Biochem. Biophys. Res. Commun. 46 (1972) 150–154.
[5] J.A. Zahn, D.M. Arciero, A.B. Hooper, A.A. Dispirito, Eur. J. Biochem. 240 (1996) 684–691.
[6] T.M. Schmidt, A.A. DiSpirito, Arch. Microbiol. 154 (1990) 453–458.
[7] M.J. Romao, M. Archer, in: A. Messerschmidt, R. Huber, T. Poulos, K. Wieghardt (Eds.), Handbook of Metalloproteins, John Wiley & Sons, Chichester, UK, 2001, pp. 44–54.
[8] T.E. Meyer, G. Cheddar, R.G. Bartsch, E.D. Getzoff, M.A. Cusanovich, G. Tollin, Biochemistry 25 (1986) 1383–1390.
[9] R. Cross, J. Aish, S.J. Paston, R.K. Poole, J.W. Moir, J. Bacteriol. 182 (2000) 1442–1447.
[10] Z. Ren, T. Meyer, D.E. McRee, J. Mol. Biol. 234 (1993) 433–445.
[11] B.C. Finzel, P.C. Weber, K.D. Hardman, F.R. Salemme, J. Mol. Biol. 186 (1985) 627–643.
[12] T.H. Tahirov, S. Misaki, T.E. Meyer, M.A. Cusanovich, Y. Higuchi, N. Yasuoka, J. Mol. Biol. 259 (1996) 467–479.
[13] T.H. Tahirov, S. Misaki, T.E. Meyer, M.A. Cusanovich, Y. Higuchi, N. Yasuoka, Nat. Struct. Biol. 3 (1996) 459–464.
[14] T.H. Tahirov, S. Misaki, T.E. Meyer, M.A. Cusanovich, Y. Higuchi, N. Yasuoka, Acta Cryst. D53 (1997) 658–664.
[15] L.M. Ramirez, H.L. Axelrod, S.R. Herron, B. Rupp, J.P. Allen, K.A. Kantardjieff, J. Chem. Cryst. 33 (2003) 413–424.
[16] M. Archer, L. Banci, E. Dikaya, M.J. Romao, J. Biol. Inorg. Chem. 2 (1997) 611–622.
[17] A.J. Dobbs, B.F. Anderson, H.R. Faber, E.N. Baker, Acta Cryst. D52 (1996) 356–368.
[18] D.M. Lawson, C.E. Stevenson, C.R. Andrew, R.R. Eady, EMBO J. 19 (2000) 5661–5671.
[19] M.A. Cusanovich, Biochim. Biophys. Acta 236 (1971) 238–241.
[20] N. Shibata, S. Iba, S. Misaki, T.E. Meyer, R.G. Bartsch, M.A. Cusanovich, Y. Morimoto, Y. Higuchi, N. Yasuoka, J. Mol. Biol. 284 (1998) 751–760.
[21] R. Weiss, A. Gold, J. Terner, Chem. Rev. 106 (2006) 2550–2579.
[22] A. Ehrenberg, M.D. Kamen, Biochim. Biophys. Acta 102 (1965) 333–340.
[23] T. Horio, M.D. Kamen, Biochim. Biophys. Acta 48 (1961) 266–286.
[24] M.D. Kamen, T. Kakuno, R.G. Bartsch, S. Hannon, Proc. Natl. Acad. Sci. USA 70 (1973) 1851–1854.
[25] J. Rawlings, P.J. Stephens, L.A. Nafie, M.D. Kamen, Biochemistry 16 (1977) 1725–1729.
[26] M.H. Emptage, R. Zimmermann, L.J. Que, E. Munck, W.D. Hamilton, W.H. Orme-Johnson, Biochim. Biophys. Acta 495 (1977) 12–23.

[27] G.N. La Mar, J.T. Jackson, R.G. Bartsch, J. Am. Chem. Soc. 103 (1981) 4405–4410.
[28] M.H. Emptage, A.V. Xavier, J.M. Wood, B.M. Alsaadi, G.M. Moore, R.C. Pitt, R.J.P. Williams, R.P. Ambler, R.G. Bartsch, Biochemistry 20 (1981) 58–64.
[29] J.T. Jackson, G.N. La Mar, R.G. Bartsch, J. Biol. Chem. 258 (1983) 1799–1805.
[30] I. Bertini, F. Briganti, R. Monnanni, A. Scozzafava, P. Carlozzi, R. Materassi, Arch. Biochem. Biophys. 282 (1990) 84–90.
[31] L. Banci, I. Bertini, P. Turano, M. Vicens Oliver, Eur. J. Biochem. 204 (1992) 107–112.
[32] I. Bertini, G. Gori, C. Luchinat, A.J. Vila, Biochemistry 32 (1993) 776–783.
[33] M.M. Maltempo, T.H. Moss, M.A. Cusanovich, Biochim. Biophys. Acta 342 (1974) 290–305.
[34] M.M. Maltempo, J. Chem. Phys. 61 (1974) 2540–2547.
[35] M.M. Maltempo, Biochim. Biophys. Acta 379 (1975) 95–102.
[36] M.M. Maltempo, T.H.Q. Moss, Quart. Rev. Biophys. 9 (1976) 181–215.
[37] T. Yoshimura, S. Suzuki, H. Iwasaki, S. Takakuwa, Biochem. Biophys. Res. Commun. 144 (1987) 224–279.
[38] T. Yoshimura, S. Suzuki, T. Kohzuma, H. Iwasaki, S. Shidara, Biochem. Biophys. Res. Commun. 169 (1990) 1235–1241.
[39] F. Monkara, S.J. Bingham, F.H.A. Kadir, A.G. McEwan, A.J. Thomson, A.G.P. Thurgood, G.R. Moore, Biochim. Biophys. Acta 1100 (1992) 184–188.
[40] S. Fujii, T. Yoshimura, H. Kamada, K. Yamaguchi, S. Suzuki, S. Shidara, S. Takakuwa, Biochim. Biophys. Acta 1251 (1995) 161–169.
[41] M.M. Maltempo, T.H. Moss, K. Spartalian, J. Chem. Phys. 73 (1980) 2100–2106.
[42] M.M. Maltempo, Biochim. Biophys. Acta 434 (1976) 513–518.
[43] G.N. La Mar, J.T. Jackson, L.B. Dugad, M.A. Cusanovich, R.G. Bartsch, J. Biol. Chem. 265 (1990) 16,173–16,180.
[44] T.C. Strekas, T.G. Spiro, Biochim. Biophys. Acta 351 (1974) 237–245.
[45] R. Barakat, T.C. Strekas, Biochim. Biophys. Acta 679 (1982) 393–399.
[46] R.G. Bartsch, Methods Enzymol. 23 (1971) 344–363.
[47] S. Benini, W.R. Rypniewski, K.S. Wilson, S. Ciurli, Acta Cryst. D54 (1998) 284–287.
[48] Z. Otwinowski, W. Minor, Methods Enzymol. 276 (1997) 307–325.
[49] B.W. Matthews, J. Mol. Biol. 33 (1968) 491–497.
[50] Collaborative Computational Project N, Acta Cryst. D50 (1994) 760–763.
[51] J. Navaza, Acta Cryst. A50 (1994) 157–163.
[52] G.N. Murshudov, A.A. Vagin, A. Lebedev, K.S. Wilson, E.J. Dodson, Acta Cryst. D55 (1999) 247–255.
[53] G.N. Murshudov, A.A. Vagin, E.J. Dodson, Acta Cryst. D53 (1997) 240–255.
[54] R.A. Engh, R. Huber, Acta Cryst. A47 (1991) 392–400.
[55] T.A. Jones, J.Y. Zou, S.W. Cowan, M. Kjeldgaard, Acta Cryst. A47 (1991) 110–119.
[56] V.S. Lamzin, K.S. Wilson, Methods Enzymol. 277 (1997) 269–305.
[57] R.A. Laskowski, M.W. MacArthur, D.S. Moss, J.M. Thornton, J. Appl. Crystallogr. 26 (1993) 283–291.